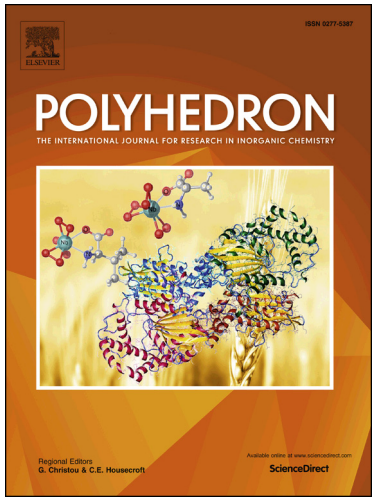

Synthesis, structure, catechol oxidase and phenoxazinone synthase mimicking activity of a manganese(III) Schiff base complex $[Mn(HL)_2(CH_3OH)_2][Mn(HL)_2(N_3)_2]$

Nandita Sarkar, Klaus Harms, Shouvik Chattopadhyay

PII: S0277-5387(17)30691-5
DOI: https://doi.org/10.1016/j.poly.2017.10.029
Reference: POLY 12893

To appear in: *Polyhedron*

Received Date: 31 July 2017
Accepted Date: 27 October 2017

Please cite this article as: N. Sarkar, K. Harms, S. Chattopadhyay, Synthesis, structure, catechol oxidase and phenoxazinone synthase mimicking activity of a manganese(III) Schiff base complex $[Mn(HL)_2(CH_3OH)_2][Mn(HL)_2(N_3)_2]$, *Polyhedron* (2017), doi: https://doi.org/10.1016/j.poly.2017.10.029

Synthesis, structure, catechol oxidase and phenoxazinone synthase mimicking activity of a manganese(III) Schiff base complex $[Mn(HL)_2(CH_3OH)_2][Mn(HL)_2(N_3)_2]$

Nandita Sarkar[a], Klaus Harms[b] and Shouvik Chattopadhyay[a,*]

[a]*Department of Chemistry, Inorganic Section, Jadavpur University, Kolkata 700 032, India, E-mail:* ***shouvik.chem@gmail.com***

[b]*Fachbereich Chemie, Philipps-Universität Marburg, Hans-Meerwein-Strasse, D-35032 Marburg, Germany.*

Abstract

An ionic coordination complex of manganese(III), $[Mn(HL)_2(CH_3OH)_2][Mn(HL)_2(N_3)_2]$ (where H_2L = 1-(5-hydroxy-3-oxapentyliminomethyl)-3-ethoxyphenol), has been synthesized. Elemental analyses and spectroscopic techniques have been performed to characterize the complex. The structure has been determined by the single crystal X-ray diffraction study. The complex consists of a complex cation, $[Mn(HL)_2(CH_3OH)_2]^+$ and a complex anion, $[Mn(HL)_2(N_3)_2]^-$. Each of which has six-coordinate centrosymmetric manganese(III) centre and is significantly elongated due to the Jahn-Teller distortion at the d^4 manganese(III) center. Hirshfeld surface analysis was used for visually analyzing intermolecular interactions in the solid state structure of the complex. Fingerprint plot reveals the percentage of intermolecular contacts (O···H, C···H and N···H) in it. The complex is found to show efficient catalytic activity towards aerial oxidation of 3,5-di-*tert*-butylcatechol (3,5-DTBC) and *o*-aminophenol with K_{cat} values 292.44 and 215.58 h^{-1} respectively.

Keywords: Jahn-Teller distortion; bidentate phenolic Schiff base ligand; hydrogen bonding; C···H-π interaction; Kinetics.

1. Introduction

The catalytic oxidation of organic substrates by metalloenzymes is of considerable interest due to the possible applications in a large variety of important synthetic, industrial and biological processes [1-11]. The synthesis and reactivity study of transition metal complexes, as model complexes for such metalloenzymes is of particular interest for the development of bio-inspired catalysts for oxidation reactions. One such enzyme that plays a key role in these reactions is catechol oxidase, a type-III copper protein. Catechol oxidase, in contrast to tyrosinase, catalyzes exclusively the oxidation of catechols to the corresponding o-quinones without acting on monophenols [12]. It consists of a binuclear copper center, where each copper is coordinated by three histidine nitrogen atoms. Catechol oxidase mimicking activity of several manganese(II), manganese(III) and manganese(IV) complexes are reported in literature [13-19]. The enzyme phenoxazinone synthase, is a type-II copper-containing oxidase (subunit molecular mass 88,000, 3.7 Cu per subunit) [20] and is naturally found in the bacterium *Streptomyces antibioticus*. This enzyme catalyzes the oxidative coupling of two molecules of substituted *o*-aminophenol to the phenoxazinone chromophore in the final step in the biosynthesis of actinomycin D [21], which is used clinically to treat Wilm's tumor, gestational choriocarcinoma, and other tumors [22-24]. Only a few manganese(III) containing model systems have been reported to exhibit phenoxazinone synthase mimicking activity [25-29].

In this paper, synthesis and characterization of a new manganese(III) complex, $[Mn(HL)_2(CH_3OH)_2][Mn(HL)_2(N_3)_2]$ have been reported. X-ray structure clearly shows that

manganese(III) is present in both cationic and anionic units of the complex. The complex shows good catalytic activity for the aerial oxidation of 3,5-DTBC to 3,5-DTBQ (3,5-di-*tert*-butylbenzoquinone) and *o*-aminophenol to 2-aminophenoxazine-3-one. The details inspection of catalytic activity shows that the complex cation takes part in the reaction and not the complex anion.

2. Experimental Section

All chemicals were of reagent grade and used as purchased from Sigma-Aldrich without further purification.

Caution!!! Although no problems were encountered in this work, metal complexes containing organic ligands in the presence of perchlorate and azides are potentially explosive. Only a small amount of the material should be prepared and it should be handled with care.

2.1. Syntheses of Schiff base ligand, 1-(5-hydroxy-3-oxapentyliminomethyl)-3-ethoxyphenol (H_2L) and corresponding manganese(III) complex $[Mn(HL)_2(CH_3OH)_2][Mn(HL)_2(N_3)_2]$

The Schiff base ligand, H_2L, was prepared by refluxing 3-ethoxysalicylaldehyde (152 mg, 1 mmol) with 2-(2-aminoethoxy)ethanol (0.1 mL, 1 mmol, density = 1.048 g/mL at 25 °C(lit.)) in methanol solution (10 mL) for ca. 1h. The ligand was not isolated and used directly for the preparation of the complex. A methanol solution (5 mL) of manganese(II) perchlorate hexahydrate (370 mg, 1 mmol) was added to the methanol solution of H_2L (1 mmol) and within few minutes colour of the solution changes to deep brown. The resulting mixture was refluxed for ca. 1 h followed by the addition of methanol-water (2:1) solution (5 mL) of sodium azide (130 mg, 2 mmol). It was then cooled and kept for slow evaporation in open atmosphere.

Dark brown coloured block shape single crystals, suitable for X-ray diffraction, were obtained after few days which were collected via filtration then dried in open atmosphere.

Yield: 514 mg (81%, based on manganese). Anal. Calc. for $C_{54}H_{80}Mn_2N_{10}O_{18}$ (FW 1267.15): C, 51.18; H, 6.36; N, 11.05%. Found: C, 51.1; H, 6.2; N, 11.2%. IR (KBr, cm^{-1}): 1620 ($\nu_{C=N}$), 2031 (ν_{N3}). UV-Vis, λ_{max} (nm) (ε_{max}(L mol^{-1} cm^{-1})) (CH_3CN): 672 (618), 470 (6.9×10^3), 314 (2.99×10^4), 227 (6.59×10^4). Magnetic moment = 6.8 μ_B

2.2. Physical measurements

Elemental analyses (carbon, hydrogen and nitrogen) were performed using a PerkinElmer 240C elemental analyzer. IR spectra in KBr (4500-500 cm^{-1}) were recorded with a PerkinElmer Spectrum Two spectrophotometer. Electronic spectra (800-200 nm) were recorded on a PerkinElmer Lambda 35 UV-visible spectrophotometer. The magnetic susceptibility measurement was done with an EG & PAR vibrating sample magnetometer (model 155) at room temperature and diamagnetic corrections were performed using Pascal's constants [30]. Electro-spray ionization mass spectra were recorded with Waters QTOF Micro YA263 mass spectrometer.

2.3. X-ray crystallography

A suitable single crystal of the complex was used for data collection using a 'Bruker D8 QUEST area detector' diffractometer equipped with graphite-monochromated Mo K_α radiation, a graded multilayer mirror monochromator (λ= 0.71073 Å) and a PHOTON-100 detector using an oil-coated shock-cooled crystal at 110(2) K. Absorption effects were corrected semi-empirical using multiscanned reflections (SAINT V8.35A (Bruker AXS Inc., 2015)) [31]. Cell constants were refined using 9901 of observed reflections of the data collection. The structure was solved

by direct methods by using the program XT V2014/1 (Bruker AXS Inc., 2014) [32] and refined by full matrix least squares procedures on F^2 using SHELXL-2017/1 (Sheldrick, 2017) [33]. The non-hydrogen atoms have been refined anisotropically, carbon bonded hydrogen atoms were included at calculated positions and refined using the 'riding model' with isotropic temperature factors at 1.2 times (for CH_3 groups 1.5 times) that of the preceding carbon atom. CH_3 groups were allowed to rotate about the bond to their next atom to fit the electron density. Oxygen bonded hydrogen atoms were located and allowed to refine isotropically. The other programs used were APEX3 [34], DIAMOND [35]. Crystallographic data and refinements details of the complex are given in Table 1. Important bond lengths and angles are listed in Table 2.

4. Hirshfeld surface Analysis

Molecular Hirshfeld surfaces and the associated 2D-fingerprint were calculated using the CrystalExplorer 3.0 program which accepted a structure input file in CIF format [36]. The Hirshfeld surface analysis is a powerful method for gaining information about different intermolecular interactions, and to identify and quantify these interactions. Hirshfield surfaces are defined implicitly by the simple equation $w(\mathbf{r}) = 0.5$, where the weight function $w(\mathbf{r})$ is given by

$$\boldsymbol{w(r)} = \sum_{\boldsymbol{i \in molecule}} \boldsymbol{\rho_i}(\mathbf{r}) / \sum_{\boldsymbol{i \in crystal}} \boldsymbol{\rho_i}(\mathbf{r})$$

Where $\rho_i(\mathbf{r})$ is a spherical atomic electron distribution located at the i th nucleus [37-38]. The weight function represents the ratio between the sum of spherical atom electron densities for a molecule (the promolecule) and the same sum for the entire crystal (the procrystal), and therefore the Hirshfeld surface envelops that region of space surrounding a particular molecule in

a crystal where the electron distribution of the promolecule exceeds that due to any other molecule. A typical Hirshfeld surface is represented by tens of thousands of surface points obtained by triangulation, and two parameters (d_e and d_i) convey information about relevant contact distances from each point. These two parameters defined as, d_e = the distance from the point to the nearest nucleus external to the surface and d_i = the distance to the nearest nucleus internal to the surface. The normalized contact distance (d_{norm}) based on d_e and d_i was given by

$$\mathbf{d_{norm}} = \frac{(\mathbf{d_i} - \mathbf{r_i^{vdw}})}{\mathbf{r_i^{vdw}}} + \frac{(\mathbf{d_e} - \mathbf{r_e^{vdw}})}{\mathbf{r_e^{vdw}}}$$

Where r_i^{vdw} and r_e^{vdw} are the van der Waals radii of the atoms. The value of d_{norm} could be negative or positive depending on intermolecular contacts, being shorter or longer than the van der Waals separations. The parameter d_{norm} displayed a surface with a red-white-blue colour scheme, where bright red spots highlighted shorter contacts, white areas represented contacts around the van der Waals separation, and blue regions were devoid of close contacts. For a given crystal structure and set of spherical atomic electron densities, the Hirshfeld surface was unique [39] and it was this property that suggested the possibility of gaining additional insight into the intermolecular interaction of molecular crystals.

2.5. Catalytic and Kinetic studies

The catalytic activity of the complex towards the aerial oxidations of 3,5-di-*tert*-butyl catechol (3,5-DTBC) and *o*-aminophenol involved in this investigation to their respective products [3,5-di-*tert*-butylbenzoquinone (3,5-DTBQ) and 2-aminophenoxazine-3-one] were followed spectrophotometrically in a 1 cm quartz cell at 298 K. Specific wavelengths characteristic of the product were chosen to follow the progress of the reaction (3,5-DTBQ, ~400

nm; 2-aminophenoxazine-3-one, ~433 nm). In typical experiments, 10^{-5} M solution of the complex in acetonitrile was added to solutions with varying concentrations (10^{-4} M to 10^{-3} M) of substrate (3,5-DTBC/ *o*-aminophenol) in acetonitrile. The complex was mixed with at least ten equivalents of substrate to maintain the pseudo-first order conditions to determine the dependence of rate on the substrate concentration and various kinetic parameters. The kinetics of oxidations was determined by the method of initial rates.

3. Results and discussion

3.1. Synthesis of $[Mn(HL)_2(CH_3OH)_2][Mn(HL)_2(N_3)_2]$

The Schiff base ligand, H_2L, was prepared by 1:1 condensation of 2-(2-aminoethoxy)ethanol with 3-ethoxysalicylaldehyde. A methanol solution of H_2L was reacted with manganese(II) perchlorate hexahydrate followed by the addition of sodium azide which produced the complex, $[Mn(HL)_2(CH_3OH)_2][Mn(HL)_2(N_3)_2]$. In this case, the deprotonation is favoured by the hydroxide ions produced by the reduction of O_2 during the aerial oxidation of manganese(II) to manganese(III). The formation of the complex is shown in scheme 1.

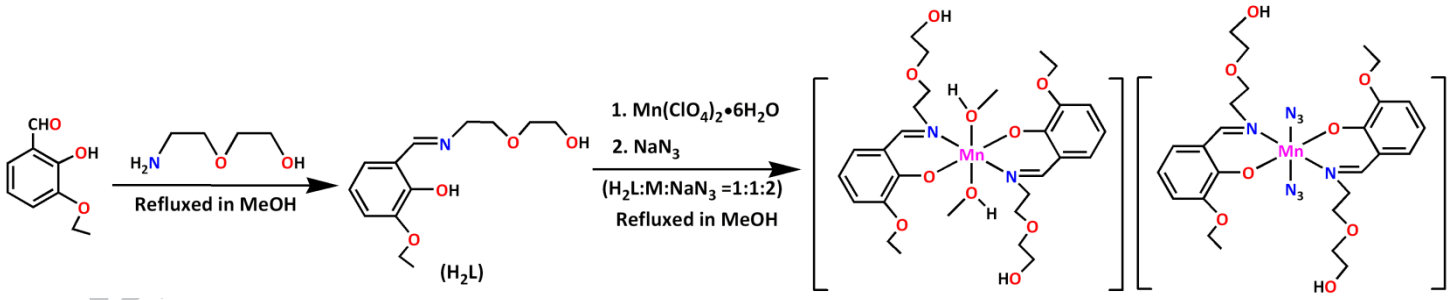

Scheme 1: Synthesis of the complex.

3.2. Structure description of $[Mn(HL)_2(CH_3OH)_2][Mn(HL)_2(N_3)_2]$

The X-ray crystal structure determinations reveal that the complex crystallizes in the triclinic space group $P\bar{1}$. A perspective view of the ionic coordination complex along with the metal centre coordinated atom numbering scheme is shown in Figure 1. It consists of one cationic complex $[Mn(HL)_2(CH_3OH)_2]^+$ and one anionic complex $[Mn(HL)_2(N_3)_2]^-$. Each complex ion contains a crystallographic inversion center at the central manganese(III). In both cationic and anionic complexes, manganese(III) ions exhibit highly distorted octahedral coordination spheres, with two nitrogen atoms and two oxygen atoms of the tetradentate Schiff base [Mn(2)-N(108) = Mn(2)-N(108)^b : 2.033 Å; Mn(2)-O(101) = Mn(2)-O(101)^b : 1.865 Å in cationic complex and Mn(1)-N(8) = Mn(1)-N(8)^a : 2.052 Å; Mn(1)-O(1) = Mn(1)-O(1)^a : 1.867 Å in anionic complex where ^{a} = 2-x,1-y,2-z; ^{b} = 1-x,1-y,1-z] defining the equatorial plane. The axial positions are occupied by two oxygen atoms [O(117) and O(117)^b] of methanol molecules in cationic complex and two nitrogen atoms of azides [N(17) and N(17)^a] in anionic complex. The longer values of axial bonds compared to equatorial bonds are indicative of tetragonal elongations as a result of the Jahn-Teller distortion, expected for high-spin manganese(III) complexes with d^4 configuration (Mn(2)-O(117) = Mn(2)-O(117)^a : 2.225 Å and Mn(1)-N(17) = Mn(1)-N(17)^b: 2.270 Å) [40-43].

The hydrogen atom, H(117), attached with oxygen atom, O(117), shows hydrogen bonding interaction with oxygen atom, O(14) with following donor-hydrogen, donor…acceptor and acceptor….hydrogen distances: O(117)-H(117) = 0.80(5) Å; O(117)···O(14) = 2.635(4) Å; H(117)···O(14) = 1.85(5) Å. The donor-hydrogen···acceptor angle is ∠O(117)-H(117)···O(14) = 170(4)°. Hydrogen atom, H(14), attached with oxygen atom, O(14), form hydrogen bonding

interaction with symmetry related oxygen atom, $O(114)^b$ (^{b} =1-x,1-y,1-z) with O(14)-H(14) = 0.70(5) Å; H(14)···$O(114)^b$ = 2.02(5) Å; O(14)···$O(114)^b$ = 2.711(4) Å and ∠O(14)-H(14)···$O(114)^b$ = 173(5)°. Another hydrogen atom, H(114), attached with oxygen atom, O(114), shows hydrogen bonding interaction with symmetry related nitrogen atom, $N(17)^c$ (^{c} = x,y,-1+z) with O(114)-H(114) = 0.80(4) Å; H(114)···$N(17)^c$ = 1.94(4) Å; O(114)···$N(17)^c$ = 2.734(4) Å and ∠O(114)-H(114)···$N(17)^c$ = 170(4)°. Due to this hydrogen bonding interactions a 2D hydrogen bonded structure is formed (Figure 2).

The hydrogen atom, H(11J), attached with C(116), is involved in C–H···π interaction with a symmetry related (1-x,2-y,1-z) phenyl ring, Cg(3) = [C(101)-C(102)-C(103)-C(104)-C(105)-C(106)] with H(11J)···Cg(3) = 2.73 Å; C(116)···Cg(3) = 3.548(3) Å and ∠C(116)-H(11J)···Cg(3) = 141°. Hydrogen atom, H(13A), attached with C(13), shows C–H···π interaction with a symmetry related (1-x,1-y,1-z) phenyl ring, Cg(3) = [C(101)-C(102)-C(103)-C(104)-C(105)-C(106)] with H(13A)···Cg(3) = 2.54 Å; C(13)···Cg(3) = 3.447(3) Å and ∠C(13)-H(13A)···Cg(3) = 153°. Another hydrogen atom, H(15A), attached with C(15), shows C–H···π interaction with a symmetry related (2-x,2-y,2-z) phenyl ring, Cg(6) = [C(1)-C(2)-C(3)-C(4)-C(5)-C(6)] with H(15A)···Cg(6) = 2.73 Å; C(15)···Cg(6) = 3.538(3) Å and ∠C(15)-H(15A)···Cg(6) = 140°. Due to these C–H···π interactions a 2D structure is formed (Figure 3).

3.3. IR, electronic spectra and magnetic moment

The $\bar{\nu}_{C=N}$ stretching vibration of manganese-bound imine functionality is observed at 1620 cm^{-1} [44]. Strong and sharp band at 2031 cm^{-1} indicates the presence of nitrogen bonded azide moiety in the complex [45]. Sharp bands of lower intensity in the range of 2974-2872 cm^{-1} due to alkyl C-H bond stretching vibrations are customarily noticed in the IR spectrum of the

complex [46]. A broad band at ~3435 cm^{-1} in the IR spectrum of the complex is attributed to the presence of hydrogen bonded OH groups [47]. Stretching frequency at ~1123 cm^{-1} indicates the presence of aliphatic ether moiety in ligand pendant arms [48].

The electronic absorption spectrum of the complex was measured in acetonitrile. The complex shows absorption shoulder at ~672 nm for the manganese(III) based spin allowed d-d transition. Bands around 400-200 nm region are likely to be of charge transfer origin. Absorption bands at ~227 and ~314 nm are assigned to intraligand $\pi \rightarrow \pi^*$ and $n \rightarrow \pi^*$ transitions respectively. Band at ~470 nm may be attributed to the ligand to metal charge transfer (LMCT) transitions [49-50].

The formulation of the complex as manganese(III) complex is supported by the room temperature solid state magnetic moments close to ~6.8 μ_B. This value is expected for magnetically non-coupled high spin manganese(III) complexes (d^4, S = 2) [51-53].

3.4. Hirshfeld Surface analysis

Hirshfeld surfaces of the complex, mapped over a 3D d_{norm} (range of -0.1 to 1.5 Å), shape index and curvedness, are illustrated in Figure 4(A). The surfaces are shown as transparent to allow visualization of the molecular moiety around which they are calculated. The intermolecular interactions mentioned in structure description part, are summarized effectively in the spots with the large circular depressions (deep red) visible on the d_{norm} surfaces indicative of hydrogen bonding contacts and other weak contacts (C–H$\cdots\pi$/ $\pi\cdots\pi$). The intermolecular interactions appear as distinct spikes in the 2D fingerprint plots (Figures 4(B)). Complementary regions are visible in the fingerprint plots where one molecule acts as donor ($d_e < d_i$) and the other as an acceptor ($d_e > d_i$). The fingerprint plots can be decomposed to highlight particular

atoms pair close contacts. For the complex, the H···H interaction has the highest contribution of the total Hirshfeld surface. Despite the high share of this interaction, its role in the stabilization of structure is quite small in magnitude because this interaction is between the same species [54]. C···H/H···C close contacts, attributed to C–H···π interactions, comprise 15.6% of the total surface. The high proportion of C···H/H···C interactions and its appearing as bright red spots on d_{norm} surface of the complex, is indicating the importance of this interaction in the structure of the complex. The proportion of O···H/H···O and N···H/H···N interactions comprise 11% and 11.1% of the Hirshfeld surfaces for the complex respectively.

3.4. Catalytic experiments

3.4.1. Catechol oxidation like activity (oxidation of 3,5-DTBC)

The oxidation of 3,5-DTBC by O_2 to the corresponding 3,5-DTBQ is catalyzed by the complex in acetonitrile. The overall stoichiometry is given by the equation:

$$\mathbf{3,5\text{-}DTBC + 0.5O_2 \rightarrow 3,5\text{-}DTBQ + H_2O}$$

To measure this catalytic activity, the complex (10^{-5} M) was treated with the substrate (3,5-DTBC) varying the concentration from 10^{-4} M to 10^{-3} M in acetonitrile (CH_3CN) at 25°C under aerobic conditions. The oxidation product, 3,5-DTBQ, is considerably stable and has a strong absorption at λ_{max}~ 400 nm. A blank experiment without catalyst under identical conditions does not show significant growth of the band at λ_{max}~ 400 nm. The increase of intensity of the absorption spectra due increasing 3,5-DTBQ, is shown in Figure 5(A).

The electrospray ionization mass (ESI-MS positive) spectral characterization was performed with 1:50 mixture of the complex with 3,5-DTBC in acetonitrile to elucidate the mechanistic pathway of the oxidation of 3,5-DTBC. Important peak in Figure 6, at *m/z* = 243.0836 corresponding to quinone sodium aggregates $[3,5\text{–DTBQ-Na}]^+$ which suggest the

completion of oxidation of 3,5-DTBC. Peak at *m/z* = 254.0860 indicates the presence of $[H_2L\text{-}H]^+$. The probable mechanism of the oxidation of 3,5-DTBC is shown in Scheme 2.

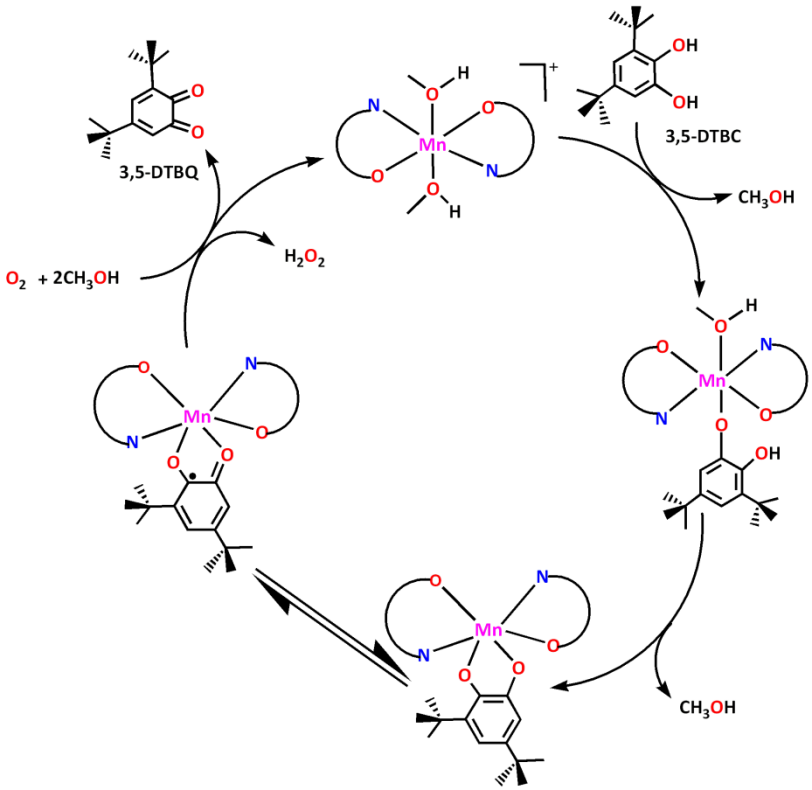

Scheme 2: Probable mechanistic pathway showing the formation of 3,5-DTBQ.

3.4.2. Phenoxazinone synthase like activity (oxidation of o-aminophenol)

The *o*-aminophenol system may be regarded as a functional model of phenoxazinone synthase, which is involved in the biosynthesis of Actinomycin D (AD), a naturally occurring antineoplastic agent, from the *o*-aminophenol derivative A (shown below):

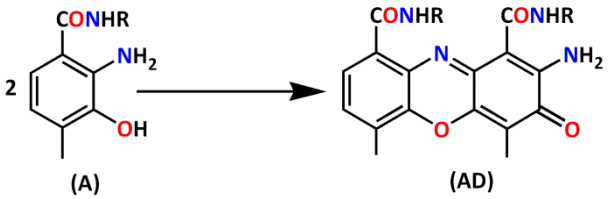

In this case the catalytic activity of the complex for air oxidation of *o*-aminophenol was investigated by mixing a fixed concentration (10^{-5} M) of catalyst with various concentration of

substrate (10^{-4} M to 10^{-3} M).The reaction product is 2-aminophenoxazine-3-one shows its characteristic wavelength at λ_{max}~ 433 nm. A blank experiment without catalyst under identical conditions does not show significant growth of the band at λ_{max}~ 433 nm. The spectral profile is given in Figure 5(B).

To illuminate the mechanistic pathway of the oxidation of *o*-aminophenol, mass spectral ionization of 1:50 mixture of the complex with *o*-aminophenol was performed. Peak at *m/z* = 215.0038 indicates the formation of [phenoxazinone-H]$^+$ and also suggest the completion of mechanistic cycle of the oxidation of *o*-aminophenol. The mass spectrum is given in Figure 7. The probable mechanistic pathway is shown in Scheme 3.

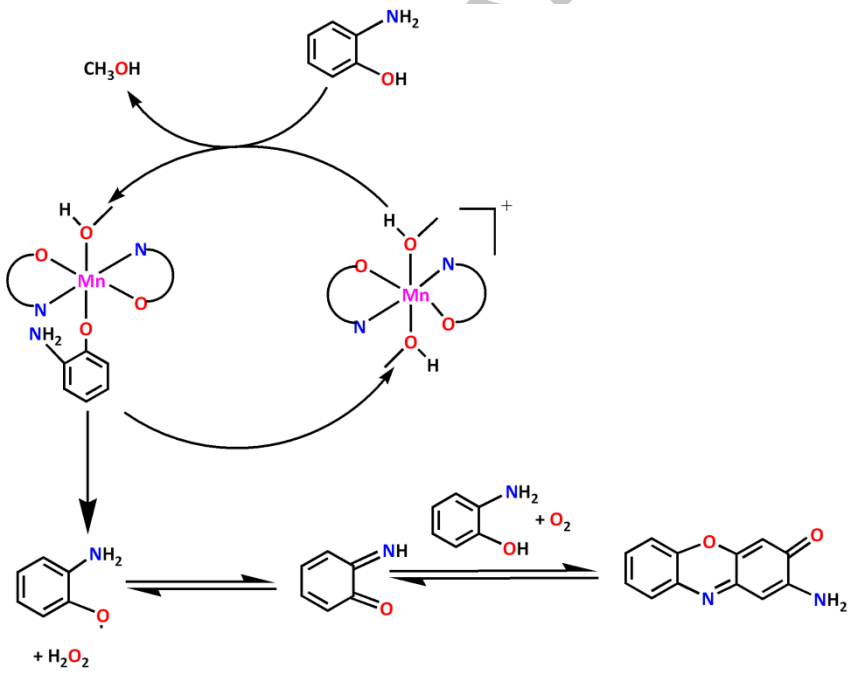

Scheme 3: Probable mechanistic pathway showing the formation of 2-aminophenoxazine-3-one

3.4.3 Kinetic overview

In the kinetic studies, the Briggs-Haldane scheme is used, which considers the formation and dissociation reactions of the enzyme-substrate complex, ES, and its decomposition reaction, forming the products and regenerating the enzyme.

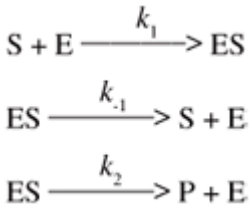

Applying this kinetic scheme to the steady state approximation for the concentration of the enzyme-substrate adducts the famous Michaelis-Menten equation for the initial reaction rate was obtained (equation 1).

$$\text{Rate (time}^{-1}) = V_{max}[S]_0/([S]_0 + K_M) \text{ - - - - - - - - (1)}$$

Plots of Eq. 1 for kinetic studies of air oxidations of 3,5-DTBC and *o*-aminophenol catalyzed by the complex show rectangular hyperbolic nature which finally tends towards a saturation curve. This proofs that the first order rate kinetics followed by the substrates. The initial rate constants, V (min^{-1}), are obtained directly from the slope of the plot of $\log[A_\infty - A_0/(A_\infty - A_t)]$ vs. time which is a straight line passing through origin. According to the Eq. 1, the limiting rate at high substrate concentration $[S]_0$ is designated as V_{max} ($V_{max} = k_{cat}[E]_0$)

$$\text{Rate}/[E]_0 = k_{cat}[S]_0/([S]_0 + K_M) \text{ - - - - - - - - - (2)}$$

Where $[E]_0$ is now k_{cat}. From Eq. 2 the following double reciprocal, linearized eq. is obtained.

$$[E]_0/\text{ Rate} = (K_M/ k_{cat})\ 1/[S]_0 + 1/k_{cat} \text{ - - - - - - - - - - (3)}$$

Plots of 1/Rate vs. $1/[S]_0$ was used to determine the kinetic parameters, $\mathbf{V_{max}}$ i.e maximum reaction velocity, $\mathbf{K_M}$ i.e. Michaelis constant and $\mathbf{K_{cat}}$ i.e. turnover number. All related plots of these two catalytic activities by the complex are shown in Figures 8 and 9. All kinetic parameters values are given in Table 3.

4. Conclusion

A new manganese(III) complex with salen type N_2O_2 donor Schiff base has been synthesized and characterized. The structure of the complex has been determined by single crystal X-ray crystallography analysis, which reveals that it consists of one cationic complex and one anionic complex. In each complex, there is a high spin manganese(III), the structure of which is elongated octahedral as a result of Jahn-Teller distortion. Hirshfeld surface analysis was used for analyzing intermolecular interactions in the crystal structure. Fingerprint plots reveal the percentage of intermolecular contacts (O···H, C···H and N···H) in the complex. C···H/H···C interactions are the highest (15.6%) among all other interactions. This signifies the importance of the C···H-π interaction in the solid state assembly of the complex. The catechol oxidase and phenoxazinone synthase mimicking activities of the complex were monitored spectrophotometrically which shows K_{cat} values 292.44 and 215.58 h^{-1} respectively. Tentative mechanistic pathways of both catalytic activities are proposed based on mass spectral data. Only the complex cation is found to show both catalytic activities. The complex cation contains two neutral methanol molecules which are easily replaceable with the respective substrates (3,5-DTBC for catechol oxidase mimicking activity and *o*-aminophenol for phenoxazinone synthase mimicking activity). Whereas the complex anion contains anionic azide co-ligands and it is

always easier to replace a neutral molecule than a charged species (N_3^- in the anionic complex). Therefore substrates prefer to attack in the complex cation than the complex anion one.

Acknowledgments

N.S. thanks the UGC, India, for awarding a Junior Research Fellowship (Sr. No. 2061410290, Ref. No.: 22/06/2014(i)EU-V, dated 7.08.2015).

Appendix A. Supplementary data

CCDC 1564558 contains the supplementary crystallographic data for the complex. These data can be obtained free of charge via http://www.ccdc.cam.ac. uk/conts/retrieving.html or from the Cambridge Crystallographic Data Centre, 12 Union Road, Cambridge CB2 1EZ, UK; fax: (+44) 1223-336-033; or e-mail: deposit@ccdc.cam.ac.uk .Supplementary data associated with this article can be found, in the online version, at http://dx.doi.org/10.1016/j.ica.2016.11.009.

References

[1] K. D. Karlin, Y. Oultneh, Prog. Inorg. Chem. 35 (1987) 219-327.

[2] R. A. Sheldon, J. K. Kochi, Metal-Catalyzed Oxidation of Organic Compounds. Academic Press, New York (1981).

[3] J. Haggin, Chem. Eng. News, 71 (1993) 23-27.

[4] L. I. Simándi, Catalytic Activation of Dioxygen by Metal Complexes, Kluwer Academic Publishers, Dordrecht, Boston, London (1992).

[5] E. I. Solomon, U. M. Sundaram, T. E. Machonkin, Chem. Rev. 96 (1996) 2563-2606.

[6] E. B. Meunier, Biomimetic Oxidations Catalyzed by Transition Metal Complexes, Imperial College Press, London (2000).

[7] J. Reedijk, Bioinorganic Catalysis, Dekker, New York (1993).

[8] M. Costas, M. P. Mehn, M. P. Jensen, Jr. L. Que, Chem. Rev. 104 (2004) 939-986.

[9] E. A. Lewis, W. B. Tolman, Chem. Rev. 104 (2004) 1047-1076.

[10] R. Hage, A. Lienke, Angew. Chem. 118 (2006) 212-229.

[11] N. Duran, E. Esposito, Appl. Catal. B 28 (2000) 83-99.

[12] M. Trémoliéres, J. B. Bieth, Phytochemistry 23 (1984) 501-505.

[13] A. Guha, K. S. Banu, A. Banerjee, T. Ghosh, S. Bhattacharya, E. Zangrando, D. Das, J. Mol. Catal. A 338 (2011) 51-57.

[14] J. Kaizer, G. Barath, R. Csonka, G. Speier, L. Korecz, A. Rockenbauer, L. Parkañyi, J. Inorg. Biochem. 102 (2008) 773-780.

[15] J. Kaizer, R. Csonka, G. Barath, G. Speier, Trans. Met. Chem. 32 (2007) 1047-1050.

[16] A. Majumder, S. Goswami, S. R. Batten, M. S. E. Fallah, J. Ribas, S. Mitra, Inorg. Chim. Acta 359 (2006) 2375-2382.

[17] K. S. Banu, T. Chattopadhyay, A. Banerjee, M. Mukherjee, A. S. Bhattacharya, G. K. Patra, E. Zangrando, D. Das, Dalton Trans. (2009) 8755-8764.

[18] S. Mukherjee, T. Weyhermüller, E. Bothe, K. Wieghardt, P. Chaudhuri, Dalton Trans. (2004) 3842-3853.

[19] G. Blay, I. Fernandez, J. R. Pedro, R. Ruiz, T. T. Sanchez, E. Pardo, F. Lloret, M. C. Munoz, J. Mol. Catal. A 250 (2006) 20-26.

[20] C. E. Barry, P. G. Nayar, T. P. Begley, Biochemistry 28 (1989) 6323-6333.

[21] C. E. Barry, P. Nayar, T. P. Begley, J. Am. Chem. Soc. 110 (1988) 3333-3334.

[22] U. Hollstein, Chem. Rev. 74 (1974) 625-652.

[23] E. Katz, H. Weissbach, J. Biol. Chem. 237 (1962) 882-886.

[24] E. Frei, Cancer Chemother. Rep. 58 (1974) 49-54.

[25] O. Toussaint, K. Lerch, Biochemistry 26 (1987)8567-8571.

[26] A. Panja, RSC Adv. 4 (2014) 37085–37094.

[27] A. Panja, Polyhedron 79 (2014) 258–268.

[28] M. R. Mauryaa, S. Sikarwar, T. Joseph, S. B. Halligudi, J. Mol. Cat. A: Chemical 236 (2005) 132–138.

[29] A. Panja, M. Shyamal, A. Sahab, T. K. Mandal, Dalton Trans. 43 (2014) 5443–5452.

[30] O. Kahn, Molecular magnetism, VCH, New York, 1993.

[31] SAINT, Bruker AXS Inc., Madison, Wisconsin, USA, 2015.

[32] G. M. Sheldrick, ActaCrystallogr A Found Adv. 71 (2015) 3–8.

[33] G. M. Sheldrick, Actacrystallographica. Section C, Structural chemistry 71 (2015) 3–8.

[34] APEX3, Bruker AXS Inc., Madison, Wisconsin, USA, 2015

[35] K. Brandenburg, Diamond - Crystal and Molecular Structure Visualization, Crystal Impact – H. Putz and K. Brandenburg GbR, Bonn, Germany, 2014.

[36] S. K. Wolff, D. J. Grimwood, J. J. McKinnon, D. Jayatilaka, M. A. Spackman, Crystal Explorer 3.0, University of Western Australia, Perth, 2007.

[37] M. A. Spackman, P. G. Byrom, Chem. Phys. Lett. 267 (1997) 215-220.

[38] J. J. McKinnon, A. S. Mitchell, M. A. Spackman, Chem. Eur. J. 4 (1998) 2136-2141.

[39] J. J. McKinnon, M. A. Spackman, A. S. Mitchell, Acta Crystallogr. Sect. B 60 (2004) 627–668.

[40] J. Limburg, J. S. Vrettos, R. H. Crabtree, G. W. Brudvig, J. C. de Paula, A. Hassan, A. Barra, C. Duboc-Toia, M. -N. Collom, Inorg. Chem. 40 (2001) 1698-1703.

[41] G. Assey, R. J. Butcher, Y. Gultneh, Acta Cryst. E66 (2010) m851–m852.

[42] F. Cisnetti, G. Pelosi, C. Policar, Inorg. Chim. Acta 360 (2007) 557–562.

[43] C. -G. Zhang, D. Wu, C. -X. Zhao, Transit. Metal Chem. 24 (1999) 718–721.

[44] K. Nakamoto, Infrared Spectra of Inorganic and Coordination Compounds, Fourth ed. Wiley, New York, 1986

[45] S. Sasi, M. Sithambaresan, M. R. P. Kurup, H. -K. Fun, Polyhedron 29 (2010) 2643-2650.

[46] S. Roy, S. Chattopadhyay, Inorg. Chim. Acta 433 (2015) 72–77.

[47] J. -B. Brubach, A. Mermet, A. Filabozzi, A. Gerschel, P. Roy, J. Chem. Phys. 122 (2005) 184509-184516.

[48] R. G. Snyder, G. Zerbi, Spectrochimica Acta. 23A (1967) 391 - 437.

[49] A. Bartyzel, A. A. Kaczor, J. Coord. Chem. 68 (2015) 3701-3717.

[50] P. Bhowmik, H. P. Nayek, M. Corbella, Ń. Aliaga-Alcalde, S. Chattopadhyay, Dalton Trans. 40 (2011) 7916–7926.

[51] B. J. Kennedy, K. S**.** Murray, Inorg. Chem. 24 (1985) 1552-1557.

[52] P. Seth, S. Giri, A. Ghosh, Dalton Trans. 44 (2015) 12863–12870.

[53] H. Hiraga, H. Miyasaka, R. Clérac, M. Fourmigué, M. Yamashita, Inorg. Chem. 48 (2009) 2887-2898.norg *Chem.* **2009**, *48*, 2887-289*. Chem.* **2009**, *48*, 2887-2898

[54] C. F. Matta, J. Hernández-Trujillo, T. -H. Tang, R. F. W. Bader, Chem.-Eur. J. 9 (2003) 1940–1951.

Table 1: Crystal data and refinement details of the complex

Formula	$C_{54}H_{80}Mn_2N_{10}O_{18}$
Formula Weight	1267.16
Crystal System	triclinic
Space group	$P\bar{1}$
a(Å)	9.8104(9)
b(Å)	10.5554(1)
c(Å)	14.8832(1)
α (°)	90.792(3)
β(°)	102.912(3)
γ(°)	90.604(3)
V(Å^3)	1501.9(2)
Z	1
$d_{(calc)}$ [g/cm^3]	1.401
μ [mm^{-1}]	0.499
F(000)	668
Total Reflections	26525
Unique Reflections	5426
Observed data[I > 2 σ(I)]	4749
R(int)	0.033
R1, wR2(all data)	0.0565, 0.1162
R1, wR2([I > 2 σ(I)]	0.0484, 0.1132

Table 2: Bond lengths (Å) and bond angles (°) of the complex:

Bond lengths (Å)	
Mn(1)-N(17)	2.270(3)
Mn(1)-N(8)	2.052(3)
Mn(1)-O(1)	1.867(2)
Mn(2)-O(101)	1.865(2)
Mn(2)-O(117)	2.225(2)
Mn(2)-N(108)	2.033(3)
Bond angles (°)	
N(17)-Mn(1)-N(8)	88.78(1)
N(17)-Mn(1)-N(8)[a]	91.22(1)
O(1)-Mn(1)-N(8)	90.69(9)
O(1)[a]-Mn(1)-N(8)	89.31(9)
O(1)-Mn(1)-N(17)	92.04(1)
O(1)[a]-Mn(1)-N(17)	87.96(1)
O(101)-Mn(2)-O(117)	89.38(9)
O(101)-Mn(2)-O(117)[b]	90.62(9)
O(101)-Mn(2)-N(108)	89.47(9)
O(101)-Mn(2)-N(108)[b]	90.53(9)
O(117)-Mn(2)-N(108)	89.73(1)
O(117)-Mn(2)-N(108)[b]	90.27(1)

Symmetry transformations: [a] =2-x,1-y,2-z; [b] = 1-x,1-y,1-z.

.

Table 3: Kinetic parameters of two catalytic activities activity at 25°C in CH_3CN

Catalytic activity	V_{max} **(M min^{-1})**	K_M **(M)**	K_{cat} **(h^{-1})**
Catechol oxidase activity	4.874×10^{-5}	9.434×10^{-3}	292.44
Phenoxazinone synthase activity	3.593×10^{-5}	9.836×10^{-3}	215.58

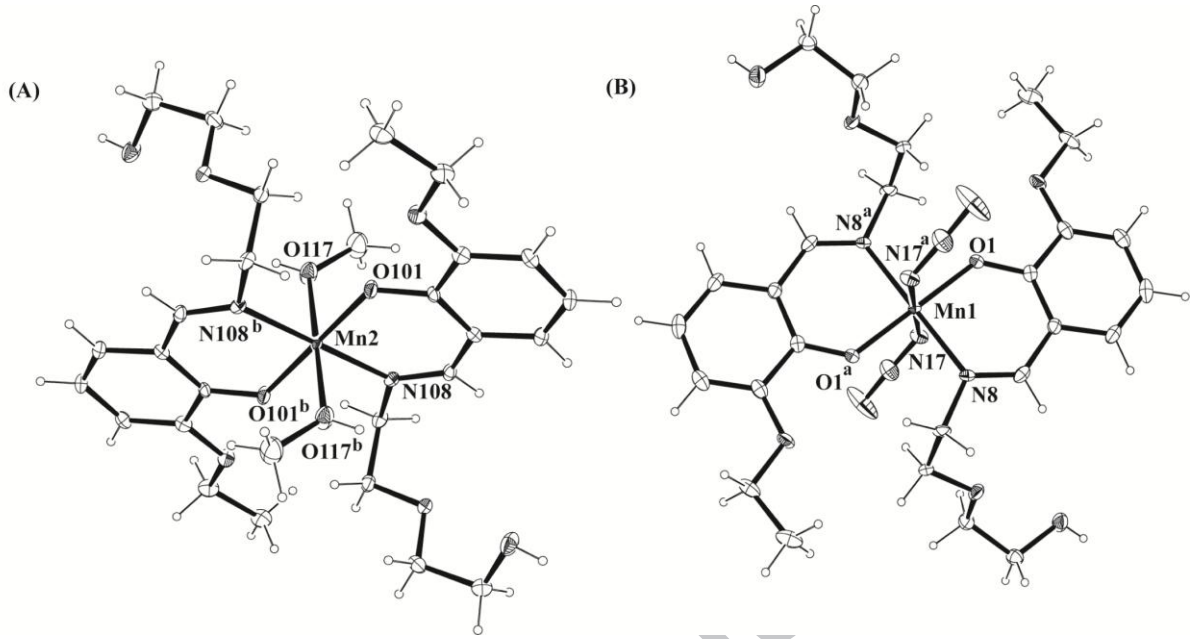

Figure 1: Perspective view of the complex with the metal centre coordinated atom numbering scheme. (**A**) Complex cation and (**B**) Complex anion. All hydrogen atoms have been deleted for clarity. Symmetry transformations: [a] = 2-x,1-y,2-z; [b] = 1-x,1-y,1-z.

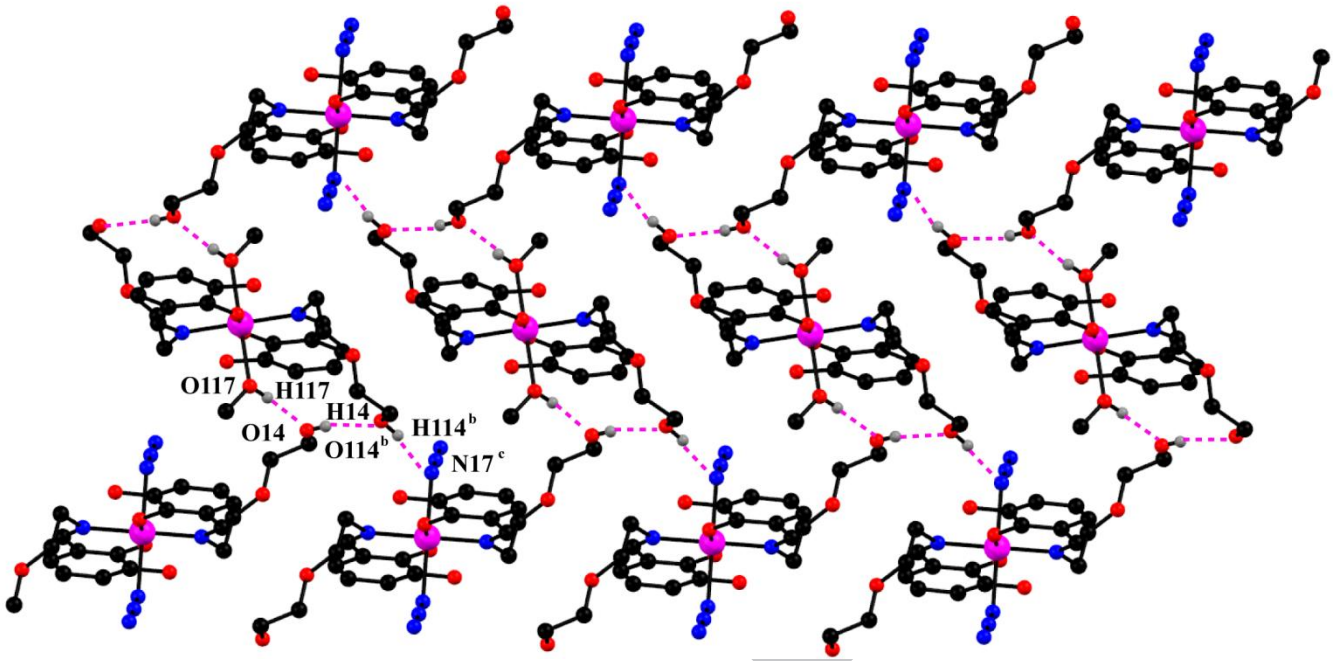

Figure 2: Supramolecular 2D structure of the complex via intermolecular hydrogen bonding interactions. Selected atoms have been omitted for clarity. Symmetry transformations [b] = 1-x,1-y,1-z; [c] = x,y,-1+z. Only the relevant atoms are labeled. Selected atoms have been omitted for clarity.

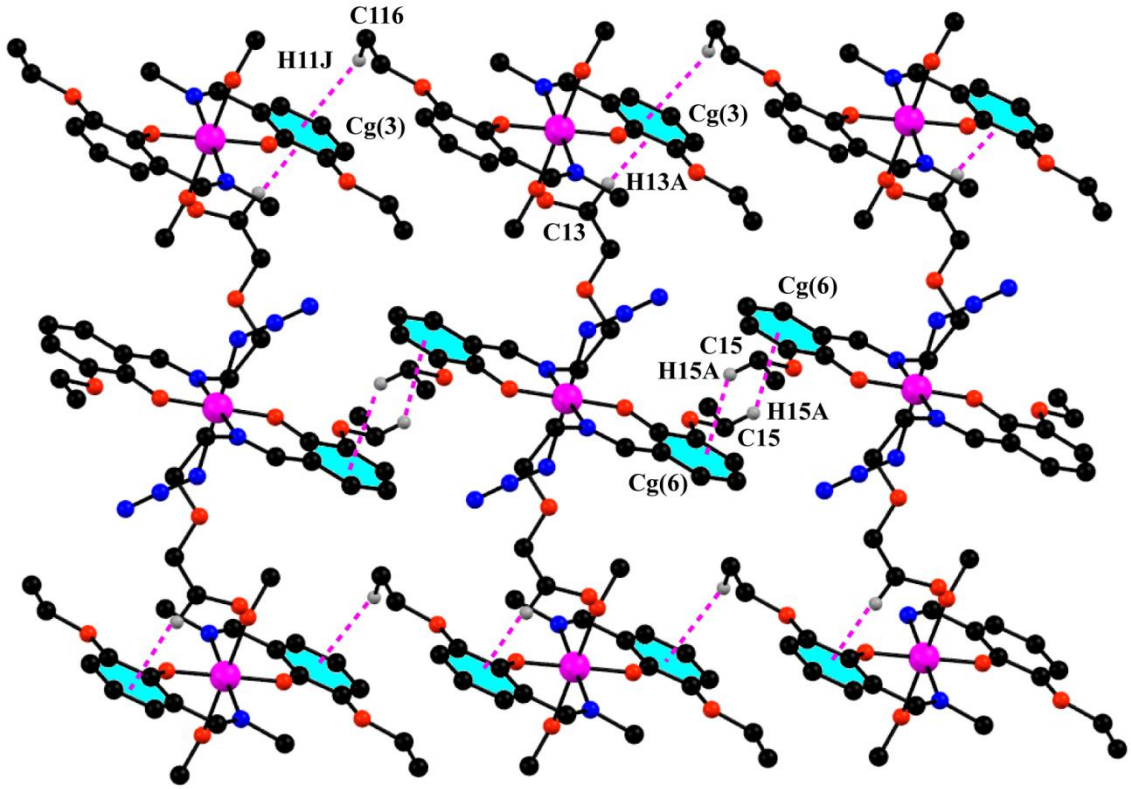

Figure 3: Supramolecular 2D structure of the complex, generated through C–H···π interactions.

Selected atoms have been omitted for clarity.

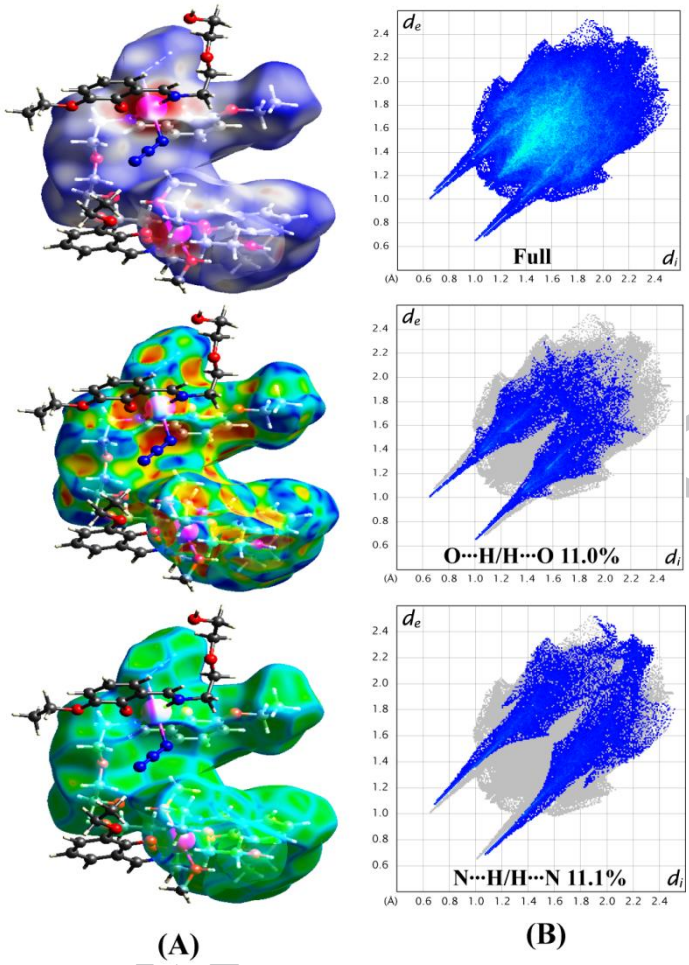

Figure 4: (A) Hirshfeld surfaces mapped with d_{norm} (top), shape index (middle) and curvedness (bottom) of the complex; **(B)** 2D Fingerprint plot of the complex shows proportions of O···H/H···O and N···H/H···N interactions comprise 11% and 11.1% of total surface of the complex.

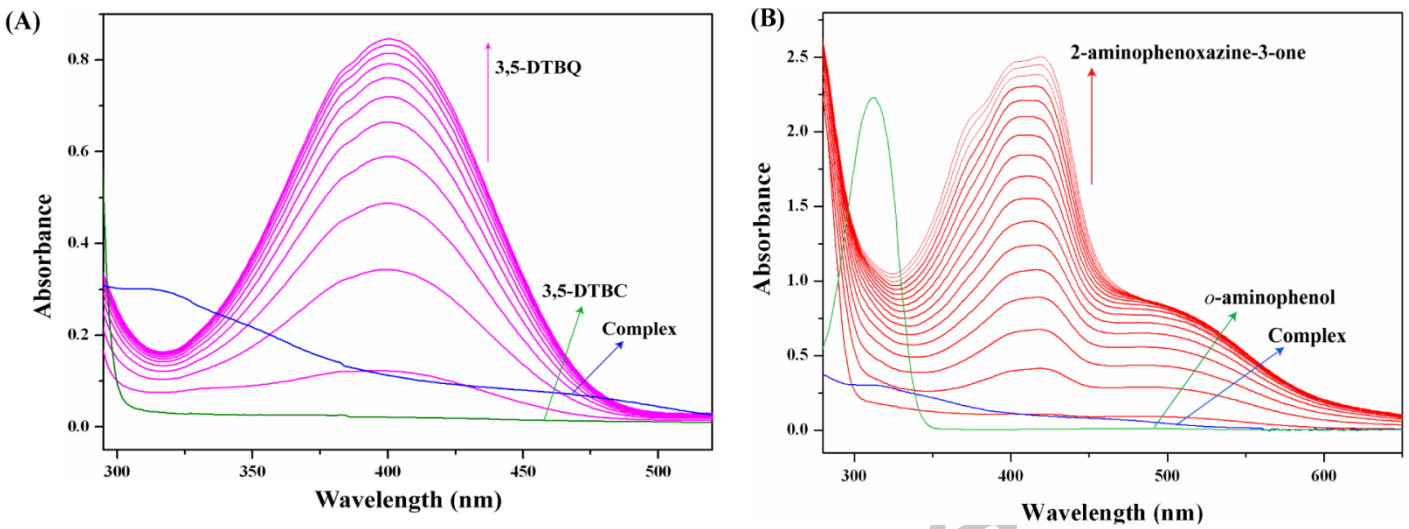

Figure 5: (**A**) UV-VIS spectral change for the aerobic oxidation of 3,5-DTBC catalyzed by the complex in CH_3CN at 25°C; (**B**) UV-VIS spectral change for the aerobic oxidation of *o*-aminophenol catalyzed by the complex in CH_3CN at 25°C.

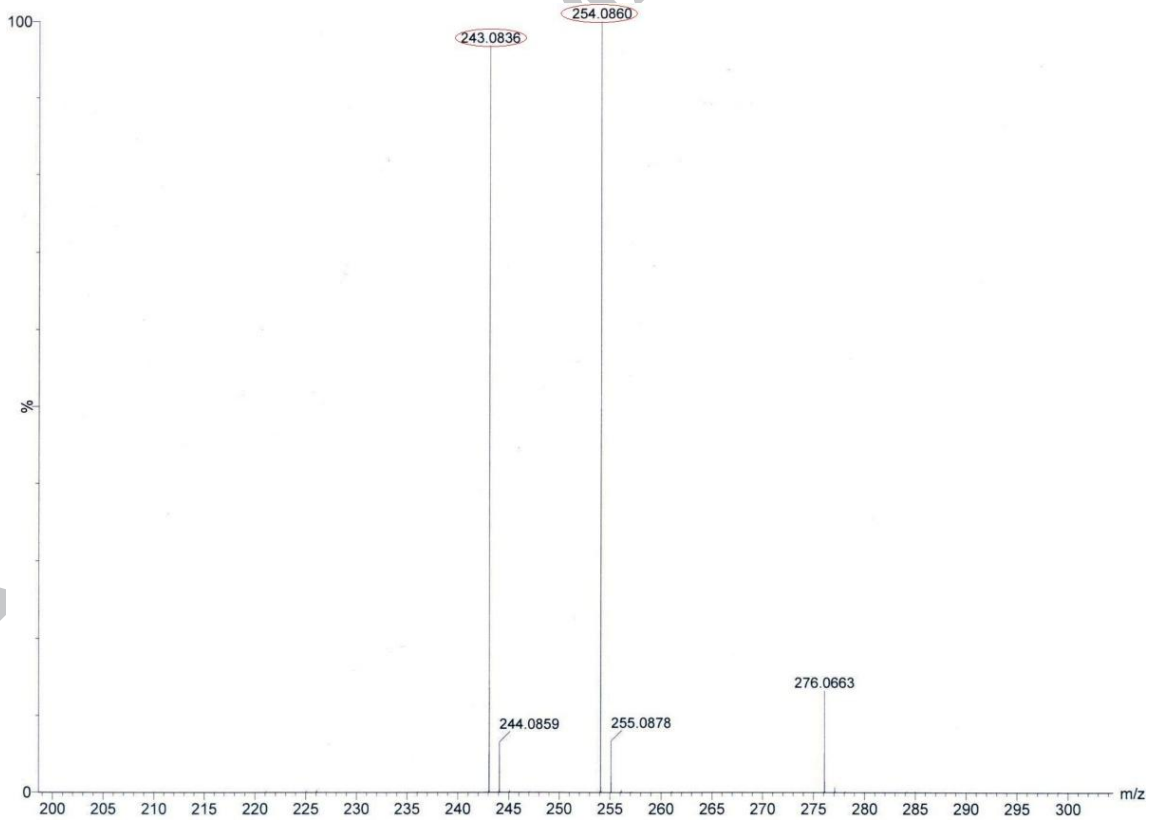

Figure 6: ESI-MS positive spectra of 1:50 mixture of the complex and 3,5-DTBC.

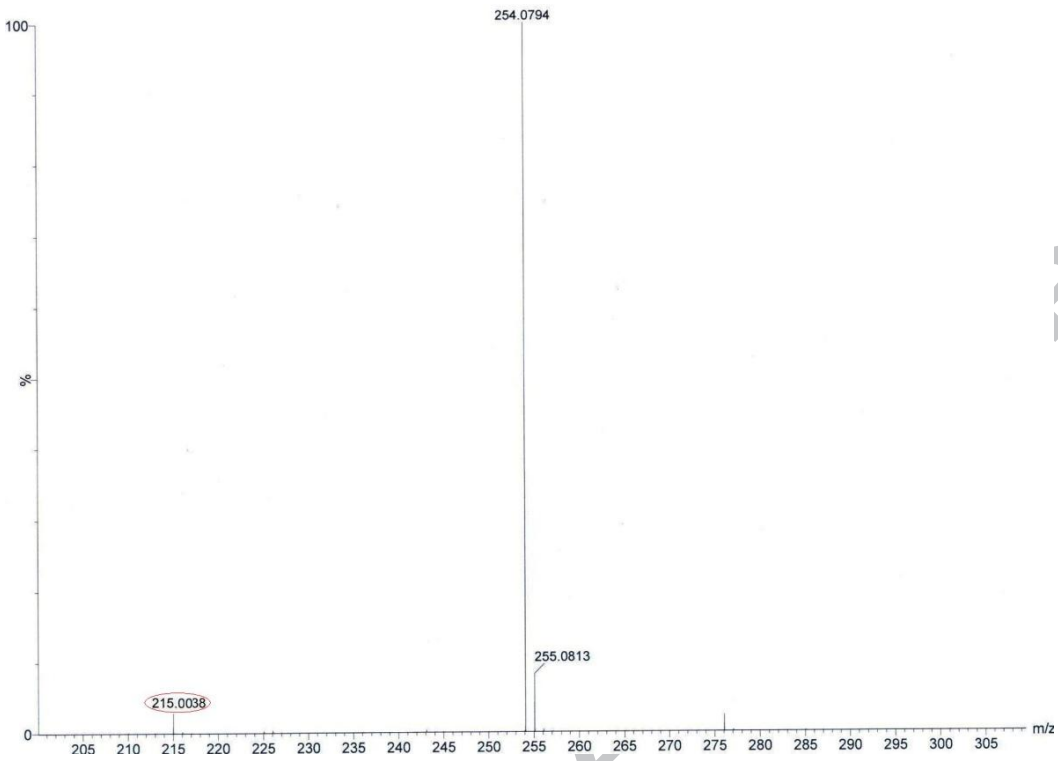

Figure 7: ESI-MS positive spectra of 1:50 mixture of the complex and *o*-aminophenol.

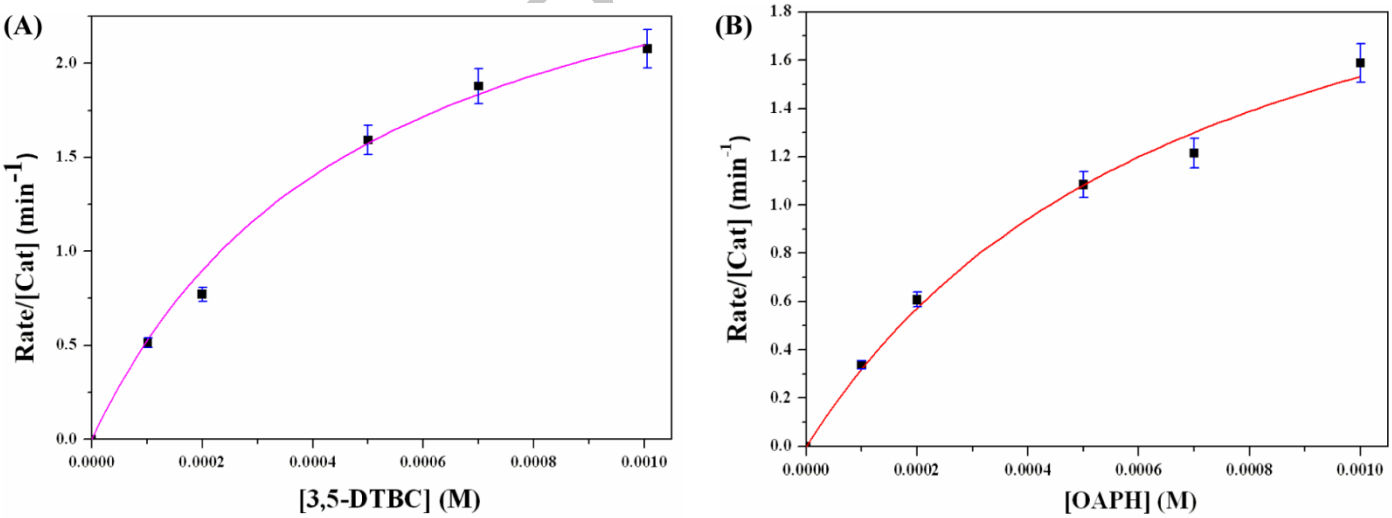

Figure 8: Michaelis-Menten plots: (A) Substrate concentration dependence on the initial rate of aerobic oxidation of 3,5-DTBC by the complex; (B) Substrate concentration dependence on the initial rate of aerobic oxidation of *o*-aminophenol by the complex.

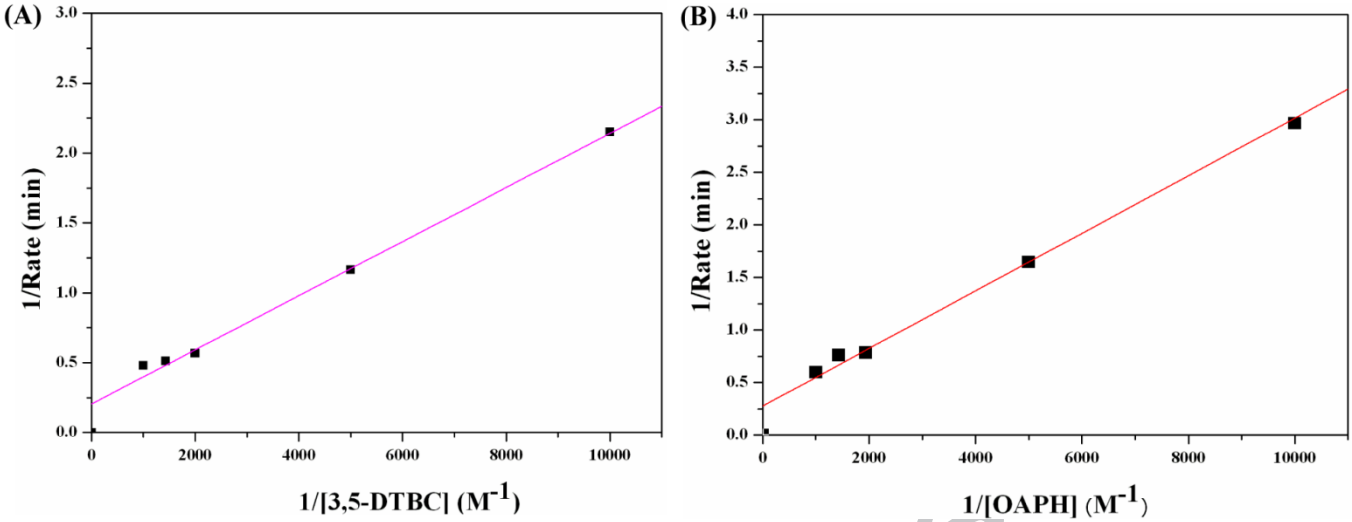

Figure 9: Plots of linearized version of Michaelis-Menten equation, in presence of **(A)** 3,5-DTBC and **(B)** *o*-aminophenol.

A new ionic coordination complex of manganese(III) with a Schiff base ligand has been synthesized and characterized using different spectroscopic techniques. The complex consists of a cationic complex and an anionic complex, each of which contains six-coordinate centrosymmetric manganese(III) centre and is significantly elongated due to the Jahn-Teller distortion at the d^4 manganese(III) center. Hirshfeld surface analysis was used for visually analyzing intermolecular interactions in the solid state structure of the complex. The complex shows good catalytic activities towards oxidations of 3,5-di-*tert*-butylcatechol and *o*-aminophenol.